frontiers | Frontiers in Chemical Engineering

ORIGINAL RESEARCH
published: 27 June 2022
doi: 10.3389/fceng.2022.849988

Modeling of a Continuous Carbonation Reactor for $CaCO_3$ Precipitation

*Johannes Tiefenthaler and Marco Mazzotti **

Separation Processes Laboratory, Department of Mechanical and Process Engineering, Institute of Energy and Process Engineering, ETH Zurich, Zurich, Switzerland

To stop global warming well below 2°C, a rapid decarbonization of our economy, including the industrial sector is required—reaching net-zero GHG emissions in 2050. CO_2 mineralization processes, capturing CO_2 from industrial point sources and trapping it as carbonate minerals, have the potential to store climate-relevant amounts of CO_2. To get there, the potential processes have to be designed and developed, with the help of a process model that can support the process scale-up and optimization. In this work, a process model describing a gas-liquid-solid continuous cristallizer for CO_2 absorption into an aqueous ammonium nitrate solution and $CaCO_3$ precipitation has been developed. It consists of the relevant material balances, of a speciation model, and a population balance equation. While several of the model parameters can be obtained from the literature, a few have been estimated by fitting a comprehensive set of experimental data presented earlier. In particular, the process quantities used for parameter estimation are the CO_2 mass transfer rate, the calcium carbonate crystallization rate, and the average particle size of the $CaCO_3$ product crystals. The accuracy of the model, particularly in reproducing mass transfer rates and average particle sizes, has been assessed. Interestingly, it has been shown that the dominating mechanism for crystal formation is primary rather than secondary nucleation. The validated model has been used to explore the effect of the different operating conditions on various key performance indicators so as to gain a deeper insight into the process performance and potential. It has been shown that the CO_2 absorption efficiency is mainly affected by the feed stoichiometry and the gas feed rate, whereas the CO_2 capture and precipitation efficiency are controlled by the liquid phase composition and the residence time; increasing the calcium concentration in the feed is obviously one way to improve the efficiency. Moreover, we could show that the particle size tends to increase with calcium concentration and to decrease with liquid feed rate and supersaturation of the solution.

Keywords: CO_2 mineralization, kinetic modelling, calcium carbonate precipitation, carbon capture and storage (CCS), precipitated calcium carbonate (PCC), CO_2 absorption

OPEN ACCESS

Edited by:
Gyorgy Szekely, King Abdullah University of Science and Technology, Saudi Arabia

Reviewed by:
Carlos A. Grande, King Abdullah University of Science and Technology (KAUST), Saudi Arabia
Matthias Kind, Karlsruhe Institute of Technology (KIT), Germany

***Correspondence:**
Marco Mazzotti
marco.mazzotti@ipe.mavt.ethz.ch

Specialty section:
This article was submitted to Separation Processes, a section of the journal Frontiers in Chemical Engineering

Received: *06 January 2022*
Accepted: *06 May 2022*
Published: *27 June 2022*

Citation:
Tiefenthaler J and Mazzotti M (2022) Modeling of a Continuous Carbonation Reactor for $CaCO_3$ Precipitation. Front. Chem. Eng. 4:849988. doi: 10.3389/fceng.2022.849988

1 INTRODUCTION

Climate change is a major threat since it sets at risk both ecosystems directly (through global warming, sea level rise, loss of biodiversity. . .) and human society indirectly (through health effects, socio-economic impact, geo-political instability. . .) (IPCC, 2019). There is scientific evidence (IPCC, 2014) and political agreement (Nations, 2015) that climate change is caused by the accumulation of green house gases (GHG) in the atmosphere, caused by the human activities that involve the use of

fossil carbon for energy generation and the release of geogenic carbon for construction materials. Hence, GHG emissions are generated across all sectors, and the related activities have been increasing the level of GHG present in the atmosphere, biosphere and oceans continuously since the industrial revolution.

Climate action requires a collaborative effort of all entities, both individuals and collectives, that cause CO_2 emissions, since local emissions have global impacts. In Paris, this collaborative strategy was framed into an agreement (Nations, 2015), with the aim to stop global warming well below 2°C. This aim implies the reduction of GHG emissions to net-zero; the economy has to undergo a rapid and complete decarbonisation in the years until 2050 (IPCC, 2018).

CO_2 is the GHG responsible for 80% of global warming (Janssens-Maenhout et al., 2017) and 20% of its total emissions are caused by the industry (IPCC, 2018). Such CO_2 emissions are often inherent to the manufacturing process—and therefore hard to avoid with conventional technologies. Moreover, they produce indispensable goods like cement, steel and chemicals. CO_2 capture, transportation, and storage (CCS) is a system of technologies, or in others words a value chain, that is designed to decarbonize industrial processes that represent large CO_2 point sources (IPCC, 2005). For the three main steps of the value chain, i.e., CO_2 capture, transportation and storage, solutions proven over many years are commercially available. The first full scale CCS chain started its operation in 1996 in Sleipner, Norway, where about 1 Mt of CO_2 per year have been captured and stored in deep saline aquifers ever since (Furre et al., 2017).

Despite the technology has been proven to operate in a robust and safe manner and the urgent need to decarbonize emission intensive industrial processes such as cement and steel manufacturing, progress in implementing CCS has been less than expected (Institute, 2019).

Implementing CCS value chains is complex, since it requires the development of policies, business models, CO_2 capture and transport infrastructure, as well as storage hubs, social acceptance, and all these elements in parallel. Thus, many stakeholders need to take a significant share of the risk—while their success is endangered if only a single element in the chain faces problems. At the same time, one element not being ready makes the chain incomplete and impossible to operate. This risk, coupled with political and business-related uncertainties delays investment decisions, which would affect the companies business model for twenty and more years to come.

As a result, the main hindering aspect of CCS is a missing business case for most locations. Unlike other technologies, CCS only avoids CO_2 emissions and does not generate any other associated value in today's market, with the exception of enhanced oil recovery, which is however in contrast not climate positive; in fact after oil is produced and utilized a larger amount of CO_2 is emitted than it is ultimately stored in the depleted reservoir. Therefore, the emission avoidance approach based on CCS does not translate into economic value as long as there is no credible carbon policy in place (Durmaz, 2018; Gardarsdottir et al., 2019).

Utilizing CO_2 to manufacture added value products can generate this required economic value. To qualify as a climate change mitigation technology, the CO_2 has to be stored for a long period of time, unless it comes either directly or indirectly (e.g. via biomass growth followed by combustion) from the atmosphere. Thus, long lived products can offer the benefit of permanent storage. However, critics argue, that the scale at which CCS deployment is required is orders of magnitudes larger than the storage potential in such products. Therefore, CO_2 capture, and utilization (CCU) might be more of a distraction rather than a viable option to mitigate climate change (Mac Dowell et al., 2017). This holds especially true for energy intensive CCU processes, e.g., the production of synthetic fuels, which require large amounts of carbon-free electricity (Abanades et al., 2017; Sutter et al., 2019; Becattini et al., 2021).

In the construction sector, CCU is especially promising, because climate relevant amounts of CO_2 can be stored permanently as carbonate minerals (Initiative, 2016). Furthermore, carbonate minerals are the thermodynamically most stable form of CO_2, hence the reaction of CO_2 to carbonate minerals is exothermic and thus generates energy instead of consuming it. Scientists have identified significant potential for CCU in the cement sector; the resulting minerals do not only store CO_2, but they can partially replace an energy and emission intensive material, i.e., clinker (Ostovari et al., 2020; Tiefenthaler, 2021).

Among the most abundant minerals used in industrial applications is calcium carbonate. Clinker and cement (Anantharaman and David, 2017), concrete (IEA, 2018), iron and steel making, pulp and paper and fillers for daily home care products require large amounts of it.

Conventionally, calcium carbonate is extracted in quarries, ground, used and incinerated or recycled (e.g., concrete recycling). Applications, which require specific properties with respect to purity, particle size and morphology use precipitated calcium carbonate (PCC), which is manufactured by calcining limestone and then re-carbonating it and precipitating it again (Mattila et al., 2014).

We envision, that PCC will in the future be produced in a GHG neutral manner. One pathway is the substitution of the calcium source limestone with industrial mineral wastes, such as slags, ashes and demolition concrete. This can mitigate feedstock related emissions. If used for construction materials, PCC can become a carbon sink. Else, if used in products, it is usually incinerated and thus can become in the best case carbon neutral. Plenty of research has been conducted in this space to develop viable processes (Sanna et al., 2014). Most promising are pH swing technologies operating with an aqueous solvent containing an ammonia salt (Mattila and Zevenhoven, 2014a). In step one, calcium is extracted from the mineral waste stream, the solid residue material is removed by filtration. In step two, the calcium rich aqueous solution is carbonated with gaseous CO_2, and PCC precipitates.

Plenty of experimental work in batch and continuous mode (Mattila and Zevenhoven, 2014b; Tiefenthaler and Mazzotti, 2021) has been conducted. To the best knowledge of the authors, comprehensive models for mineral carbonation

processes, which consider the kinetics of CO_2 absorption and of PCC precipitation are rare. Vučak (2002) provides a detailed model; however, their solvent system is considerably different than the one used here (monoethanolamine instead of an ammonium salt).

This work presents for the first time a kinetic model for CO_2 absorption into an aqueous ammonium nitrate solution, where calcium ions are present, and the ensuing precipitation of calcium carbonate, in a continuous reactive crystallization configuration. In practical applications of this process, the aforementioned solution would be prepared by contacting an ammonium nitrate solution (prepared ad hoc) with industrial mineral wastes, such as slags, ashes, and demolition concrete. The acid character of the ammonium nitrate solution enables the leaching of calcium ions from the mineral wastes. In the context of the overall process (not discussed here), the ammonium nitrate solution is recycled in a closed loop within the process itself. The relevant kinetic parameters of the system are estimated making use of experimental results obtained in a previous study (Tiefenthaler and Mazzotti, 2021).

This type of models are necessary to understand the system and to design, optimize and scale-up a process for the precipitation of PCC from waste materials. First, the thermodynamics of the system is described, upon which the kinetic model of the process is built. Afterwards, a number of empirical kinetic parameters are estimated based on experimental results, and the accuracy of the model is assessed. Finally, the model is used to gain new insights, going beyond the experimental learnings, which are presented and discussed in the **Section 4**.

2 THERMODYNAMIC MODELING

The system investigated is a crystallizer that acts as carbonation reactor and consists of a gas, a liquid and a solid phase. The gas phase contains N_2, CO_2 and moisture [NH_3 volatility at such temperatures and pH conditions can be neglected (Said et al., 2016)]; the liquid phase is an aqueous ammonium nitrate solution rich in calcium, in which CO_2 absorbs and speciates; finally the solid phase consists of the mineral $CaCO_3$ only under the conditions explored here.

A CO_2 molecule enters the system through the inlet gas stream; it is first absorbed by the aqueous solution, then it undergoes speciation reactions to form amongst others the CO_3^{2-} ion, which either precipitates with a Ca^{2+} ion to form the solid $CaCO_3$ or exits from the reactor as ion dissolved i within the mother liquor. The physical and chemical equilibria relevant for this system are as follows (Thomsen and Rasmussen, 1999; Vu č ak, 2002; Wolery, 2002; Puxty et al., 2010):

2.1 Vapor-Liquid Equilibrium

$$CO_{2,g} \overset{K_1}{\leftrightarrow} CO_{2,aq} \qquad (2-1)$$

$$H_2O_g \overset{K_2}{\leftrightarrow} H_2O_{aq} \qquad (2-2)$$

2.2 Liquid Speciation

$$CO_{2,aq} + 2NH_{3,aq} \overset{K_3}{\leftrightarrow} NH_2COO^- + NH_4^+ \qquad (2-3)$$

$$CO_{2,aq} + OH^- \overset{K_4}{\leftrightarrow} HCO_3^- \qquad (2-4)$$

$$OH^- + H^+ \overset{K_5}{\leftrightarrow} H_2O \qquad (2-5)$$

$$NH_4^+ \overset{K_6}{\leftrightarrow} NH_3 + H^+ \qquad (2-6)$$

$$CO_3^{2-} + H^+ \overset{K_7}{\leftrightarrow} HCO_3^- \qquad (2-7)$$

$$CaNO_3^+ \overset{K_8}{\leftrightarrow} Ca^{2+} + NO_3^- \qquad (2-8)$$

$$CaCO_{3,aq} + H^+ \overset{K_9}{\leftrightarrow} Ca^{2+} + HCO_3^- \qquad (2-9)$$

$$CaHCO_3^+ \overset{K_{10}}{\leftrightarrow} Ca^{2+} + HCO_3^- \qquad (2-10)$$

$$CaOH^+ + H^+ \overset{K_{11}}{\leftrightarrow} Ca^{2+} + H_2O \qquad (2-11)$$

2.3 Solid-Liquid Equilibrium

$$Ca^{2+} + CO_3^{2-} \overset{K_{12}}{\leftrightarrow} CaCO_{3,s} \qquad (2-12)$$

The geochemical equilibrium package EQ3/6 was used to identify the relevant speciation reactions; reactions which result in ionic species at very low concentrations have been neglected.

The following assumptions have been made:

- N_2 is assumed to be insoluble, and thus it does not absorb in the aqueous solution.
- The liquid water is in equilibrium with the water vapor in the gas phase.
- NH_3 is assumed to be non-volatile, since the absorption of CO_2 shifts the equilibrium towards NH_{4+}. This assumption has been tested in independent experiments which confirmed that ammonia is below the detection limit, which is in line with literature (Said et al., 2016).
- The gas and liquid phase are well mixed, i.e., both phases and its relevant intensive properties, i.e., temperature, pressure, and composition, are homogeneous in the reactor.
- CO_2 is not at equilibrium between gas and solution hence its absorption is mass transfer limited and can be described by the two film theory.
- The reaction of $CO_{2,aq}$ with NH_3 in the liquid film is considered as the rate determining step of CO_2 uptake. Consequently, all reactions in the aqueous solution can be considered to be instantaneous hence at equilibrium (Puxty et al., 2010). Moreover, evaluating the Hatta number for various operating conditions confirmed, that the reaction of $CO_{2,aq}$ with NH_3 is in the pseudo-first-order and fast reaction regime while the reaction of $CO_{2,aq}$ with OH^- lies in the very-slow to slow reaction regime. Since both occur in parallel, the reaction with NH_3 is rate determining.

- The precipitation of $CaCO_3$ is not instantaneous hence it is governed by the principles of crystallization, whereby the amount of solid mass and the crystal size distribution are controlled by the interplay between nucleation and growth, whose rates depend on the relevant driving force (agglomeration of primary particles and crystal breakage are neglected for the sake of simplicity) (Davey, 2000; Wolthers et al., 2012).
- In this work we assume representative product removal, namely that the particle size distribution of the suspension withdrawn is the same as that of the suspension in the crystallizer. We believe that this is a reasonable assumption considering that the experiments on which this modeling work is based (Tiefenthaler and Mazzotti, 2021) yielded very small particles that should yield a homogeneous suspension. A study of this particular aspect should be considered in follow up studies.

2.4 Modelling of the Liquid Speciation

The reactions in the bulk liquid (**Eqs 2-3–2-11**) are considered to be instantaneous hence they can be assumed to be at equilibrium. The corresponding chemical equilibrium conditions must be fulfilled, which can be written as:

$$K_i = \frac{\prod_j a_{j,product}}{\prod_k a_{k,educt}} \qquad (2-13)$$

$$a_j = \gamma_j c_j \qquad (2-14)$$

a_j and c_j are the activity and the concentration of the ion or molecule i; K_i is the equilibrium constant associated to the corresponding equilibrium (the equilibrium constants are reported in the **Supplementary Appendix SA**); γ_i is the activity coefficient of the ion or molecule i. Literature correlations were used to calculate the activity coefficient for NH_3 (Maeda and Kato, 1995). The activity of water and the activity coefficient of $CO_{2,aq}$ were calculated according to Wolery (2002). The activity coefficient of $CaCO_{3,aq}$ was assumed to be equal to one. The B-dot equations, which consider the dominat long-range interactions between the ions and molecules, were used to calculate the activity coefficient of charged species. A complete description and discussion of these equations can be found elsewhere (Wolery, 2002).

In addition, the electro neutrality condition has to be met:

$$\sum_i c_i z_i = 0 \qquad (2-15)$$

where the sum extends on all the ionic (charged) species and z_i corresponds to the charge of ion i. The concentration of the ionic species and molecules in solution can be used to define the following four overall concentrations in solution, which in turn will have to satisfy the overall material balances (see below):

$$c_C = c_{CO_2,aq} + c_{HCO_3^-} + c_{CO_3^{2-}} + c_{CaHCO_3^+} + c_{CaCO_3,aq} + c_{NH_2COO^-} \qquad (2-16)$$

$$c_{Ca} = c_{Ca^{2+}} + c_{CaOH^+} + c_{CaNO_3^+} + c_{CaHCO_3^+} + c_{CaCO_3,aq} \qquad (2-17)$$

$$c_{NO_3} = c_{NO_3^-} + c_{CaNO_3^+} \qquad (2-18)$$

$$c_{NH_3} = c_{NH_4^+} + c_{NH_3} + c_{NH_2COO^-} \qquad (2-19)$$

The system of equilibrium reactions is solved by making use of the geochemical equilibrium software package EQ3/6, v8.0a (Wolery, 2002). EQ3/6 is a software package for modeling geochemical interactions between aqueous solutions, solids, and gases, following principles of chemical thermodynamics and chemical kinetics, which is maintained and kept updated at the Lawrence Livermore National Laboratory[1], and has been used in earlier mineral carbonation studies (Hariharan and Mazzotti, 2017a; Hariharan and Mazzotti, 2017b; Hariharan et al., 2016; Hariharan, 2017; Werner et al., 2014a; Werner et al., 2014b). The equilibrium constant for **Eq. 2-3** is provided by Thomsen and Rasmussen (1999).

The equations above involve the concentrations of the 14 molecules and ionic species in solution: $c_{CO_2,aq}$, $c_{HCO_3^-}$, $c_{CO_3^{2-}}$, $c_{CaHCO_3^+}$, $c_{CaCO_3,aq}$, $c_{NH_2COO^-}$, $c_{Ca^{2+}}$, c_{CaOH^+}, $c_{CaNO_3^+}$, $c_{NO_3^-}$, $c_{NH_4^+}$, c_{NH_3}, c_{H^+} and c_{OH^-}. If the total concentrations of carbon c_C, of calcium c_{Ca}, of ammonium c_{NH_3}, and of nitrate c_{NO_3} are known, for instance because they are determined through the material balances for the whole system (see below) the liquid speciation equations (the nine **Eqs 2-3–2-11**) together with the definitions of the overall concentrations (**Eqs 2-16–2-19**) and the electro neutrality condition (**Eq. 2-15**) can be solved numerically to obtain the 14 unknown concentrations in solution.

3 REACTOR MODELLING

The reactor, as shown in **Figure 1**, is a continuous crystallizer, that has certain similarities to a classical MSMPR, of a total volume, V_R; it is filled with an aqueous solution of volume V_s. It is assumed that the gas, liquid and solid phases are well mixed and that the temperature is well controlled. The aqueous solution is fed at a rate Q_{in} and a liquid phase composition $c_{i,in}$. The liquid outlet flow is specified at steady state by the composition c_i, obviously the same as within the crystallizer, and the outlet flow rate Q_{out}. Gas is bubbled through the reactor's suspension at an inlet flow rate F_{in} and an inlet composition $y_{i,in}$. The gas is exiting the reactor at a flow rate F_{out} and a composition $y_{i,out}$. The CO_2 mass transfer is described by the two film theory, whereas water and water vapour are assumed to be at equilibrium. However, since the outlet gas passes through a condenser, it is assumed that the gas leaving the reactor is dry. The only solid precipitating from the solution is calcium carbonate, present either as calcite or vaterite. These solid particles are described as a population of spheres with particle size distribution (PSD) given by $f(L)$, where L is the characteristic length. The primary particles are cuboidal and spherical depending on the polymorph (calcite or vaterite, respectively), and form spherical agglomerates (Tiefenthaler and Mazzotti, 2021). Calcium carbonate precipitation is controlled by the mechanisms of nucleation and growth, and occurs at a rate that depends on their corresponding rates.

3.1 Aqueous Solution

The material balance for water in the reactor can be written as:

$$\frac{dV_s\rho}{dt} = Q_{in} - Q_{out} \qquad (3-1)$$

[1]https://www-gs.llnl.gov/energy-homeland-security/geochemistry

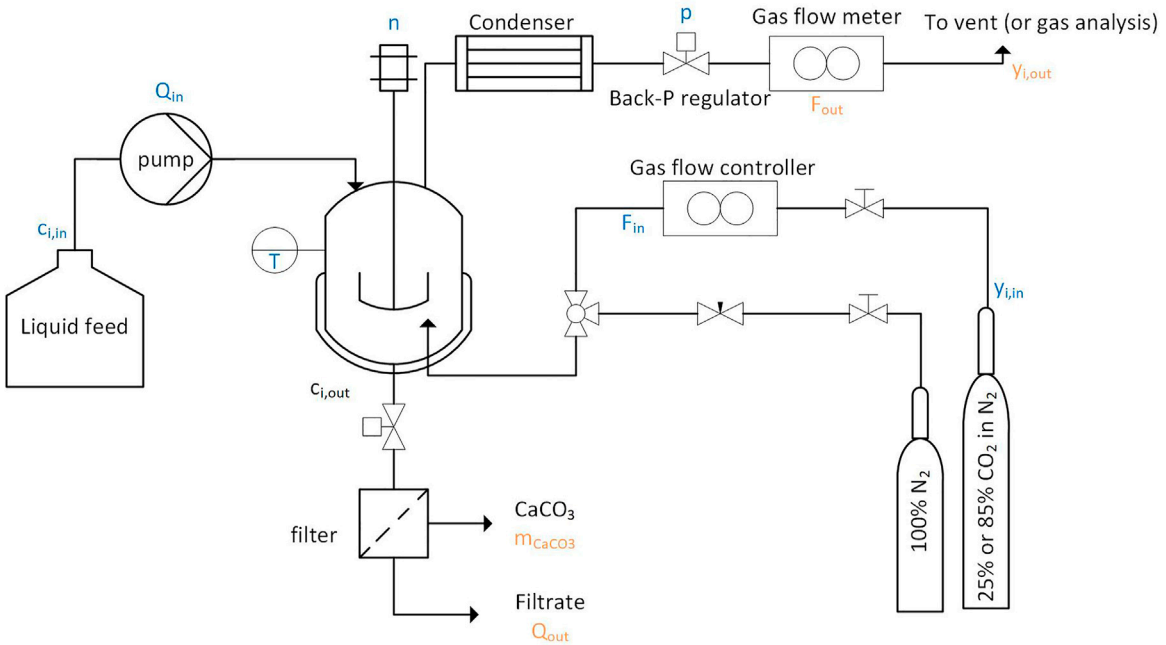

FIGURE 1 | A schematic drawing of the crystallizer modeled in the scope of this project is shown. The experimental setup is described to a greater detail in a previous publication (Tiefenthaler and Mazzotti, 2021).

The product of the liquid phase volume V_s and the liquid phase density ρ corresponds to the amount of liquid present in the reactor. The system is operated at steady state, thus Q_{in} is equal to Q_{out}, which from now are called simply Q. The mass balances for Ca, C, NH_3 and NO_3^- in the aqueous solution are:

$$V_s\rho\frac{d(c_{Ca})}{dt} = Q(c_{Ca,in} - c_{Ca}) - r_c V_s \qquad (3-2)$$

$$V_s\rho\frac{d(c_C)}{dt} = Q(c_{C,in} - c_C) + V_s(f_{MT} - r_c) \qquad (3-3)$$

$$V_s\rho\frac{d(c_{NH_3})}{dt} = Q(c_{NH_3,in} - c_{NH_3}) \qquad (3-4)$$

$$V_s\rho\frac{d(c_{NO_3})}{dt} = Q(c_{NO_3,in} - c_{NO_3}) \qquad (3-5)$$

The initial conditions for the system have to be assigned accordingly in case the calculation of the transient between start up and steady state is needed; they are not necessary for steady state simulations. The quantity c_i represents the overall concentration of component i in the aqueous solution, i.e., corresponding to the left hand side of **Eqs 2.15–2.18**.

3.2 Gas Phase

The gas phase mass balance is

$$\frac{dn_{tot}}{dt} = F_{in} - F_{out} - f_{MT}V_s \qquad (3-6)$$

The total number of moles of gas in the reactor's overhead space, n_{tot}, is calculated by the ideal gas law

$$n_{tot} = \frac{P}{RT}(V_R - V_s) \qquad (3-7)$$

P corresponds to the system pressure, R to the ideal gas constant and T to the reactor temperature. ~~The CO_2 mass balance in the gas phase is~~

$$\frac{d(n_{tot}y_{CO_2})}{dt} = F_{in}y_{CO_2,in} - F_{out}y_{CO_2,out} - f_{MT}V_s \qquad (3-8)$$

y_{CO_2} corresponds to the CO_2 mole fraction in the overhead space. The outlet gas stream is assumed to be dry, thus the CO_2 outlet concentration is calculated as follows:

$$y_{CO_2,out} = \frac{y_{CO_2}}{y_{CO_2} + y_{N_2}} \qquad (3-9)$$

y_{N_2} corresponds to the N_2 mole fraction in the overhead space of the reactor, whereby the sum of the molar gas fractions for CO_2, N_2 and H_2O in the overhead space must be equal to one.

$$\sum_i y_i = 1 \qquad (3-10)$$

The quantity f_{MT} that appears in **Eqs 3-3**, **3-7**, **3-9** couples the equations for the gas phase and for the solution and needs to be defined based on an underlying mass transfer model; this is discussed in detail in **Section 3.4**.

3.3 Solid Phase

The solid phase mass balance is

$$\frac{dn_{CaCO_3}}{dt} = r_c V_s - \frac{k_V Q\rho_c}{\rho M_{CaCO_3}}\mu_3 \qquad (3-11)$$

where n_{CaCO_3} is the number of moles of $CaCO_3$ in the reactor, k_V the volume shape factor of the crystals, equal to π/6 for spheres, ρ_c the mass density and M_{CaCO_3} the molar mass of $CaCO_3$, and μ_3 is the 3rd moment of the crystal size distribution, which must be calculated from the solution of the population balance equation, as discussed in **Section 3.5** below. The quantity r_c represents the number of moles of $CaCO_3$ that are transferred to the solid phase from solution per unit time and unit volume of the solution.

3.4 CO_2 Mass Transfer Model

A model for the gas-liquid mass transfer rate of CO_2 is adopted, which is based on the two-film theory. The rate of gaseous CO_2 absorbed by the liquid phase can be written as Levenspiel (1999a):

$$f_{MT} = k_L a_{eff} E \rho\left(c^*_{CO_2,aq} - c_{CO_2,aq}\right) \quad (3-12)$$

$$c^*_{CO_2,aq} = \frac{f_{CO_2}}{H_{CO_2}} \quad (3-13)$$

k_L is the liquid phase mass transfer coefficient, a_{eff} corresponds to the effective mass transfer area per unit volume of the suspension, E the enhancement factor, f_{CO_2} is the arithmetic mean bulk gas phase fugacity of CO_2 of the incoming and exiting gas stream, H_{CO_2} is the Henry constant of CO_2, $c_{CO_2,aq}$ is the molecular CO_2 concentration in the bulk liquid and $c^*_{CO_2,aq}$ is the concentration of molecular CO_2 at the gas—liquid interface, which is in equilibrium with the gas phase. Note that **Eq. 3.14** is the isofugacity for the CO_2 gas-liquid equilibrium referred to by **Eq. 2-1**. As a consequence of its definition, f_{MT} is given in moles of CO_2 per unit time per unit volume of the solution.

3.4.1 Enhancement Factor

The reaction of carbon dioxide with ammonia and hydroxyl ions in the liquid film enhances the CO_2 absorption. The liquid phase mass transfer coefficient has to account for this effect, hence the physical mass transfer coefficient k_L (CO_2 absorption without reaction) is multiplied by E, accounting for the reactions of **Eqs 2-3**, **2-4** (Levenspiel, 1999b; Darde et al., 2011):

$$CO_{2,aq} + 2NH_3 \overset{k_{NH_3}}{\leftrightarrow} NH_2COO^- + NH_4^+$$

$$CO_{2,aq} + OH^- \overset{k_{OH^-}}{\leftrightarrow} HCO_3^-$$

The functional form of the enhancement factor depends on the reaction regime. The reaction regime is specified by the value of the Hatta number M_H and the enhancement factor for infinitely fast reactions E_i (Darde et al., 2011).

$$M_H = \frac{\sqrt{D_{CO_2} k_A c_A}}{k_L} \quad (3-14)$$

$$E_i = 1 + \frac{D_A c_A}{2 D_{CO_2} c^*_{CO_2,aq}} \quad (3-15)$$

The Hatta number compares the rate of reaction of **Eqs 2-3**, **2-4** within the liquid film with the rate of CO_2 mass transfer through the liquid film, whereby D_{CO_2} is the diffusivity of CO_2 in the liquid phase and is calculated as follows (Versteeg and Van Swaaij, 1988)

$$D_{CO_2} = 2.35 * 10^{-6} e^{-\frac{2119}{T}} \quad (3-16)$$

D_A is the diffusivity of NH_3 molecules respectively OH^- ions in the liquid film, which can be assumed to be equal to the diffusivity of CO_2 in the liquid phase (Zeng et al., 2011). k_A is the reaction rate constant of NH_3 respectively OH^- ions with CO_2. k_{OH^-} can be determined according to the following equation (Pohorecki and Moniuk, 1988):

$$log\left(\frac{k_{OH^-}}{k^{inf}_{OH^-}}\right) = 0.221I - 0.016I^2 \quad (3-17)$$

$$k^{inf}_{OH^-} = 11.916 - \frac{2382}{T} \quad (3-18)$$

I is the ionic strength of the aqueous solution. There are a number of correlations available for k_{NH_3}. The lower bound can be calculated as follows (Pinsent et al., 1956)

$$k_{NH_3} = k_{REF} e^{-\frac{E_a}{RT}} \quad (3-19)$$

And the upper bound of the rate constant was determined as follows (Puxty et al., 2010).

$$k_{NH_3} = k_{REF}\, e^{-\frac{E_a}{R}\left(\frac{1}{T} - \frac{1}{283}\right)} \quad (3-20)$$

The average between the maximum and the minimum values of k_{NH_3} proposed in the literature (see **Table 1**) will be used for further calculations. The concentration c_A corresponds to that of the relevant reactant. For the corresponding regimes, the functional form of E is taken from a look-up table reported by Last and Stichlmair (2002). k_L and a_{eff} are system specific parameters, which have to be estimated from experimental data.

One way to identify, which of the two reactions considered enhances CO_2 mass transfer, is to compute the Hatta number and the enhancement factor for a range of operating conditions. At a CO_2 partial pressure of 0.25 bars, 25°C, k_L of $2 * 10^{-4}$ m s^{-1} (Last and Stichlmair, 2002) and a NH_3 concentration of 0.02–1 mol per kg water, the reaction regimes for both reactions were determined (not shown here). While the reaction of $CO_{2,aq}$ with OH^- ions can be found to be between the very slow and the slow reaction regime, the reaction of $CO_{2,aq}$ with NH_3 is between the fast reaction of pseudo first order and the fast reaction regime. As a result, only the presence of NH_3 enhances the CO_2 mass transfer through the gas-liquid interface. Thus, the effect of the OH^- ions on the mass transfer enhancement is neglected.

3.5 $CaCO_3$ Precipitation Model

A kinetic expression for the precipitation of $CaCO_3$ is developed. Calcium carbonate can precipitate in three main anhydrous forms: calcite, aragonite and vaterite, listed here by decreasing

TABLE 1 | Parameters for the upper and lower bound of k_{NH_3}. At 25°C, k_{NH_3} corresponds to 1,920 L mol^{-1} s^{-1}.

	k_{REF} [L mol^{-1} s^{-1}]	E_a [J mol^{-1}]
Lower bound	$11^{11.13}$	48,534.4
Upper bound	915	61,000

stability (Flaten et al., 2009). The two dominant mechanisms during precipitation are nucleation and crystal growth. In the case of the continuous process modeled here, nucleation is described according to the classic nucleation theory. To model the precipitation process of $CaCO_3$, we assume that the suspension is well mixed and that nucleation and growth are the dominant precipitation mechanisms, i.e., we have decided for the sake of simplicity to neglect the effect of agglomeration and breakage. The corresponding population balance equation can be written as (Davey, 2000; Ramkrishna, 2000; Alvarez et al., 2011):

$$\frac{\partial f}{\partial t} + G\frac{\partial f}{\partial L} + \frac{1}{\tau}(f - f_{in}) = 0 \qquad (3-21)$$

where f corresponds to the number based particle size distribution in the reactor, G to the size independent growth rate, L to the characteristic length of a particle, τ to the residence time of the suspension in the reactor, i.e., $\tau = \frac{V_s \rho_s}{Q}$, and $f_{in}(L)$ is the number based particle size distribution of the population of particles entering the reactor with the feed stream.

Since the system operates at steady state, and the feed is free of particles, **Eq. 3-21** can be simplified to:

$$G\frac{df}{dL} + \frac{1}{\tau}f = 0 \qquad (3-22)$$

With the boundary condition:

$$f(L=0) = \frac{J}{G} \qquad (3-23)$$

where J is the rate of particle nucleation and G is the rate of crystal growth. It is worth noting that for the sake of simplicity but without loss of generality we have decided not to distinguish between different polymorphs precipitating; as a consequence the driving force for nucleation and growth is expressed with respect to the crystallization of the stable polymorph, i.e., calcite.

The nucleation rate is given by the classical nucleation theory relationship (Jun et al., 2016; Reis et al., 2018):

$$J = A\exp\left(-\frac{16\pi\sigma^3 v_m^2}{3k_B^3 T^3 (\log(S))^2}\right) \qquad (3-24)$$

where S corresponds to the supersaturation with respect to calcite, σ is the surface energy, v_m represents the molecular volume of $CaCO_3$, both listed in the **Supplementary Appendix SB**. k_B is the Boltzmann. Considering the boundary conditions, the population balance, **Eq. 3-22**, can be integrated to obtain the particle size distribution:

$$f(L) = \frac{J}{G}\exp\left(-\frac{L}{G\tau}\right) \qquad (3-25)$$

One can see, that as the characteristic length of the particle approaches the size of the smallest particle ($L = 0$), the corresponding boundary condition is fulfilled. Moreover, the regularity condition is fulfilled, since the value of $f(L)$ becomes zero as the characteristic length approaches infinity (Ramkrishna, 2000).

The growth rate was assumed to be continuous in the entire range of calcite saturation values, meaning that the energy required to integrate a molecule to the solid lattice is low and that every growth unit arriving finds a site in the lattice (Davey, 2000). Thus, the growth rate can be expressed as:

$$G = k_c(S-1)^{\alpha} \qquad (3-26)$$

where k_c is the rate constant for growth, α corresponds to an empirical exponent, and S is the supersaturation with respect to calcite, which is defined as:

$$S = \sqrt{\frac{a_{CO_3^{2-}} a_{Ca^{2+}}}{K_{SP}}} \qquad (3-27)$$

where K_{SP} is the solubility product of calcite. Different growth rate models can be found in the literature, some of them are more of a theoretical nature while others more of an empirical one. Brečević (2007) developed a correlation for k_c at 25°C and for S ranging from 1 to 3 as a function of the ionic strength assuming α equal to 2. However, the discussed system operates at much higher values of supersaturation. Chen et al. (1997) claims that for gas—liquid systems, α is equal to 2.9. In addition, the surface integration is supposed to be rate limiting (also supported by others, see Nancollas and Reddy, 1971; Kazmierczak et al., 1982). Wolthers et al. (2012) develop an empirical model for k_c valid for ionic strengths ranging from 0.001–0.7 M:

$$k_c = I^{-\beta} pH^{-\gamma}\left(\frac{a_{Ca^{2+}}}{a_{CO_3^{2-}}}\right)^{-\Delta} \qquad (3-28)$$

They estimated β to be equal to 0.004, γ to be equal to 10.71 and Δ to be equal to 0.35. Furthermore, they assume α equal to 2. Nehrke et al. (2007) identified experimentally that the growth rate of calcite has a maximum at a ratio of the $a_{Ca^{2+}}$ to $a_{CO_3^{2-}}$ equal to one.

Finally, the jth moment of the crystal size distribution μ_j is defined as:

$$\mu_j = \int_0^{\infty} L^j f(L)\mathrm{d}L \qquad (3-29)$$

Using **Eq. 3-26** the integral can explicitly be calculated in the case of interest as:

$$\mu_2 = 2J\tau^3 G^2 \qquad (3-30)$$

$$\mu_3 = 6J\tau^4 G^3 \qquad (3-31)$$

Thus, the moments of the crystal size distribution are function of the residence time and of the composition of the solution, through the values of J and G that depend in turn on the supersaturation S. Moreover, **Eq. 3-11** can be solved at steady state, thus yielding the following expression for r_c:

$$r_c = \frac{6k_V \rho_c}{M_{CaCO_3}} J\tau^3 G^3 \qquad (3-32)$$

It is worth noting that the quantity r_c can be calculated independently of **Eq. 3-12** by considering that $CaCO_3$ uptake

by the solid phase occurs through crystal growth only, since new nuclei are assumed to have $L = 0$ hence zero mass. To this aim, one must calculate the product of the growth rate and the total crystal surface, which is proportional to the second moment of the particle size distribution, μ_2: the proper expression is $r_c = \frac{0.5 k_A \rho_c}{M_{CaCO_3}} G\mu_2$, which yields **Eq. 3-32** when substituting **Eq. 3-31** and considering that $\frac{k_A}{k_V} = 6$ for particles that do not change shape as they grow.

3.6 Key Operating Parameters and Key Performance Indicators

In the following, the KOPs and the KPIs, which have been developed in the scope of a previous experimental study (Tiefenthaler and Mazzotti, 2021) will be introduced as they are used in the **Section 4** of the manuscript, particularly for the comparison between simulations and experiments. The stoichiometric ratio in the feed to the reactor, ψ_F, is defined as:

$$\psi_F = \frac{F_{in} y_{CO_2,in}}{Q_{in} c_{Ca,in}} \quad (3-33)$$

The CO_2 absorption efficiency $\eta_{CO_2,abs.}$ is defined and calculated as:

$$\eta_{CO_2,abs.} = \frac{f_{MT} V_s}{F_{in} y_{CO_2,in}} \quad (3-34)$$

The product of the feed stoichiometry ψ_F and the CO_2 absorption efficiency $\eta_{CO_2,abs.}$ determines the actual ratio of the two reactants that enters the aqueous solution, ψ, which is thus:

$$\psi = \frac{f_{MT} V_s}{Q_{in}\, c_{Ca,in}} = \eta_{CO_2,abs.}\ \psi_F \quad (3-35)$$

The efficiency of the precipitation of CO_2 from the aqueous solution, $\eta_{CO_2,prec.}$, is defined as:

$$\eta_{CO_2,prec.} = \frac{r_c}{f_{MT}} \quad (3-36)$$

Finally, the CO_2 mineralization efficiency of the process with respect to CO_2, η_{CO_2}, is defined as:

$$\eta_{CO_2} = \eta_{CO_2,abs.}\, \eta_{CO_2,prec.} = \frac{r_c\, V_s}{F_{in}\, y_{CO_2,in}} \quad (3-37)$$

whilst the overall efficiency of the process with respect to calcium, η_{Ca}, is calculated as:

$$\eta_{Ca} = \frac{r_c V_s}{Q_{in}\, c_{Ca,in}} \quad (3-38)$$

Note that

$$\eta_{Ca} = \eta_{CO_2} \psi_F \quad (3-39)$$

4 RESULTS AND DISCUSSION

The experimental campaign published previously (Tiefenthaler and Mazzotti, 2021) provided insights about the effect of feed conditions on process efficiencies, but also particle related properties such as particle size and polymorph. Only experimental points at steady state have been considered for the parameter estimation. We want to assess whether the model presented in the previous sections captures the experimental trends qualitatively and/or quantitatively. If this is the case, one can use the model to develop a deeper understanding of the process, which goes beyond what observed experimentally. For this reason, this section is structured as follows. First, the system specific, empirical parameters k_L, a_{eff}, A and α are estimated based on the available experimental data set, and the quantitative performance of the model will be assessed making use of parity plots and statistic quantities such the relative mean deviation. Second, once the model accuracy is assessed, a parametric study will be conducted, exploiting the model to study the key trends in terms of process performance as function of the process operating parameters.

4.1 Estimation of Model Parameters

The process model consists of a thermodynamic model, for the speciation, of material balances and of a population balance equation, as well as of kinetics constitutive equations for mass transfer and for nucleation and growth in the crystallization process. By solving the model equations, the key quantities f_{MT}, r_c and L_{50} are calculated as function of the operating conditions. It is worth noticing that all these quantities are coupled, i.e., they are interdependent. As these quantities have been measured in our recent experimental study, the empirical model parameters k_L and a_eff as well as A and α have been estimated by minimizing the sum of the squares of the difference between the calculated and the measured values of these quantities, or in other terms the sum of the mean relative deviations (MRD), which are calculated for each measured quantity as follows:

$$MRD = \frac{1}{N_{exp}} \sum_{i=1}^{N_{exp}} \frac{\sqrt{\left(x_i^{model} - x_i^{experiment}\right)^2}}{x_i^{experiment}};\ x_i = f_{MT}\,; r_C; L_{50}; \quad (4-1)$$

where N_{exp} represents the number of experiments which are considered for estimating the parameters (exp = 16 in this work). The set of parameters reported in **Table 2** has been obtained.

The two mass transfer related parameters, k_L and a_eff, fall in the typical ranges observed in the literature. The estimated k_L is in the range for absorption processes (Last and Stichlmair, 2002).

TABLE 2 | The four estimated model parameters are listed below.

k_L	a_{eff}	A	α
[ms^{-1}]	[m^{2}m^{-3}]	[m^{-3}s^{-1}]	[-]
1.9E-4	49.2	6.5E+14	1.37

Furthermore, the interfacial surface area a_{eff} for stirred bubble tanks varies usually between 20 and 200 m^2/m^3 (Levenspiel, 1999b). The values of the two parameters in the nucleation and growth rate, A and α, must be interpreted as empirical, while the corresponding values reported in the literature have a degree of uncertainty. Therefore, we consider the values reported in the table accurate enough and acceptable (Nehrke et al., 2007).

Parity plots, shown in **Figure 2**, are used to illustrate the quantitative agreement between modelling and experimental results. They illustrate the experimental values (x-axis) of f_{MT} (**Figure 2A**), r_C (**Figure 2B**) and the volume based average particle size L_{50} (**Figure 2C**) against the output of the model (y-axis). In case the experimental results and the model were in perfect agreement, the points would lie on the solid line with an angle of 45°. The dashed and the dotted line enclose the area with a 10% and a 25% relative deviation. Note, that f_{MT}, r_c and L_{50} are obtained through three independent measurements. In case a point falls above the solid line, the model overestimates the corresponding quantity, while on the other hand, points falling below the solid line are underestimated by the model.

The experimental and modelling results for f_{MT} show a very high quantitative agreement—as visualized by **Figure 2A**. Many points fall on the solid line, none of them exhibits a MRD exceeding 10%. This holds true for the whole range, from low (5.4 mmol min^{-1} L^{-1}) to high (11.5 mmol min^{-1} L^{-1}) absorption rates.

From an experimental viewpoint, the rate of CO_2 absorption is the quantity exhibiting the highest accuracy, since it is measured directly online with a previously calibrated mass spectrometer. The empirical parameters k_L and a_{eff} are usually a function of the properties of the aqueous solution, the reactor geometry and the mixing of the aqueous solution (Laakkonen, 2005). The effect of mixing is not considered by the modelling equations. The stirring speed was kept constant in the experimental campaign. Despite the variation of the inlet gas flowrate between 12.8 and 18.5 mmol min^{-1}, the effects on the mass transfer parameters seem to be small.

Moreover, **Figure 2B** shows that the model tends to underestimate the precipitation rate in many cases by 25% or more, possibly due to the fact that the model describes growth and nucleation in a rather empirical way, for instance without accounting for the effect of the solution composition on the growth rate; these effects might be important, as described in literature (Jung et al., 2000). Despite its relative simplicity the model manages to give a quantitative description of the precipitation rate, at least of the right order of magnitude.

The third quantity, which is measured independently, i.e., L_{50}, exhibits for experiments f, n, p, t, k, o, and d a very good quantitative agreement, while the other experimental points exhibit a deviation of mostly below 25% (**Figure 2C**). This good quantitative agreement is remarkable, since certain mechanisms, such as agglomeration, which affect the particle size in the experimental campaign (Tiefenthaler and Mazzotti, 2021), are not considered by the model.

The values of MRD obtained for each measured variable support the observations made based on **Figure 2**. The quantitative agreement between experimental and modelling results is the highest for f_{MT}, which exhibits a MRD of only 2.3%, followed by L_{50} with a MRD of 16%, and finally by r_c with a MRD of 27%.

It is worth noting that we have achieved a good accuracy between simulations and experiments using a primary nucleation rate expression. This might appear to be in contradiction with the fact that the model describes a continuous crystallization process, where new $CaCO_3$ crystals are formed in the presence of already existing $CaCO_3$ crystals, i.e., under conditions where secondary nucleation should be favored. We have tried to describe the experimental results using a secondary nucleation rate equation, with the specific feature that the nucleation rate is

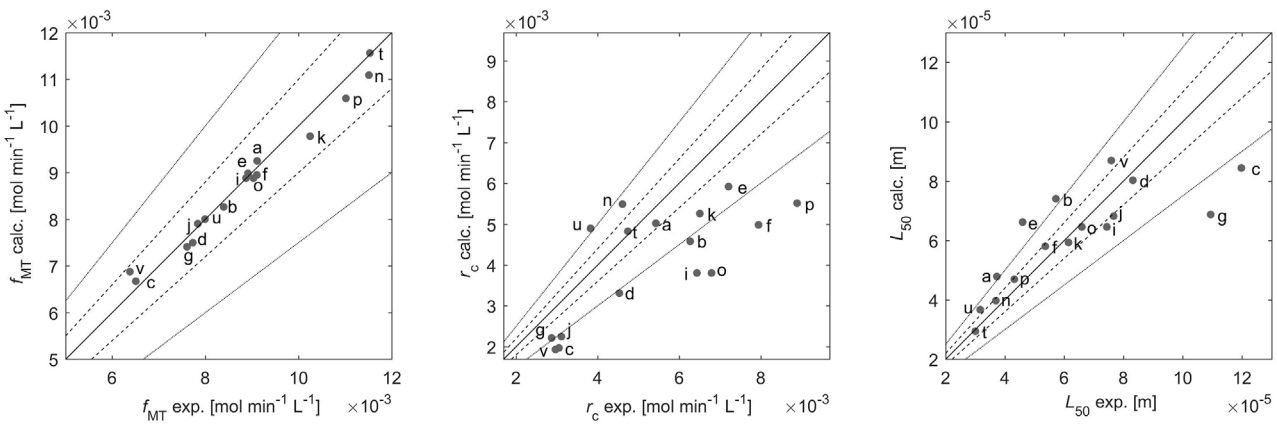

FIGURE 2 | The experimental values und the modelling results of the CO_2 absorption rate f_{MT}, the $CaCO_3$ precipitation rate r_C and the volume weighted average particle size L_{50} are visualized in parity plots.

proportional to a moment of the crystal size distribution [the third moment, as in a recent paper (Chen et al., 1997)], but we have failed, i.e., always obtaining a worse fit than what shown in **Figure 2** (results not presented here for brevity). We have rationalized this outcome by considering that primary particles are very small, thus making secondary nucleation by attrition, i.e., the dominant mechanism, unlikely, and that supersaturation is very high, thus favoring primary nucleation.

4.2 Model-Based Process Analysis

The model allows to compute process performance for any set of operating conditions, and thus helps to gain additional insights, far beyond the experimental evidence. For this reason the model was evaluated in hundreds of operating points (about 400), covering calcium concentrations from 0.2 to 0.35 molal, liquid feed rates from 9 to 36 g per minute and gas feed rates from 12.9 to 24 mmol per minute. The temperature, the CO_2 inlet concentration, and the NH_4NO_3 concentration in the feed solution were kept constant at 25 °C, 25% CO_2 and 0.7 molal, respectively.

4.2.1 Effect of Stoichiometric Feed Ratio ψ_F on the CO_2 Absorption

The stoichiometric feed ratio ψ_F determines how many moles of CO_2 per mole of calcium are fed to the reactor. Calcium carbonate precipitates to the reaction reported in **Eq. 2-12**, thus the reactants participate in the reaction with a stoichiometric ratio of one—to one. **Figures 3A,C** show the CO_2 absorption efficiency as a function of ψ_F. The variation of ψ_F in **Figure 3C** was modelled by keeping $c_{Ca,in}$ constant at 0.3 molal while varying Q_{in}. An increase in gas feed rates reduces the CO_2 absorption efficiency—as shown by the model results (solid line) and by the experimental measurements (red and blue points). Moreover, **Figure 3A** shows $\eta_{CO_2,abs.}$ computed for various operating points. Dark blue corresponds to high values of F_{in}, while yellow corresponds to the lowest values investigated. The two trends observed previously—the linear reduction of $\eta_{CO_2,abs.}$ as soon as ψ_F exceeds one, and the reduced $\eta_{CO_2,abs.}$ with increasing F_{in}, can be confirmed for a wide range of operating conditions (**Figure 3A**). The latter effect is an indication that in fact mass transfer is limiting the absorption rate, thus the process is not able to exploit the entire capacity of the solvent as more CO_2 is fed. Moreover, the results with respect to ψ are obtained by multiplying $\eta_{CO_2,abs.}$ by ψ_F. As expected, the experimental points and the model first follow a straight line with an angle of 45°, thus indicating that CO_2 absorption is almost quantitative at ψ_F values smaller than 1. At $\psi_F \sim 1$, the curve starts to saturate, and lower values of the effective stoichiometric ratios in solution, ψ , are obtained as F_{in} increases (**Figure 3B**).

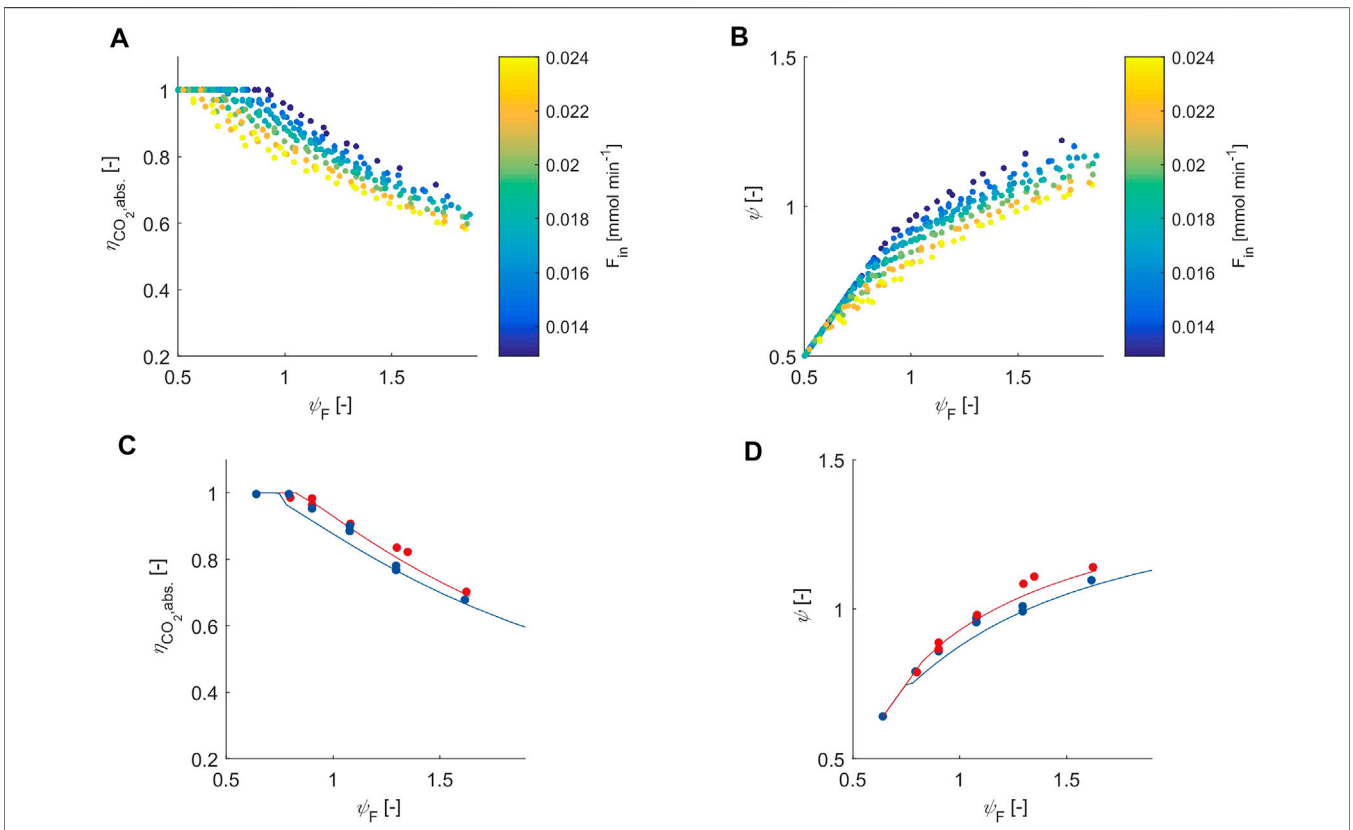

FIGURE 3 | The $\eta_{CO_2,abs.}$ and ψ are plotted as a function of ψ_F. While subplot a and b visualize simulated operating points, subplot c and d combine experimental results (filled circles) with modelling results (solid lines). Red and blue data sets correspond to results obtained at 14.8 and 18.5 mmol min^{-1}. **(A)** CO_2 absorption efficiency. **(B)** ψ vs. ψ_F. **(C)** CO_2 absorption efficiency. **(D)** ψ vs. ψ_F.

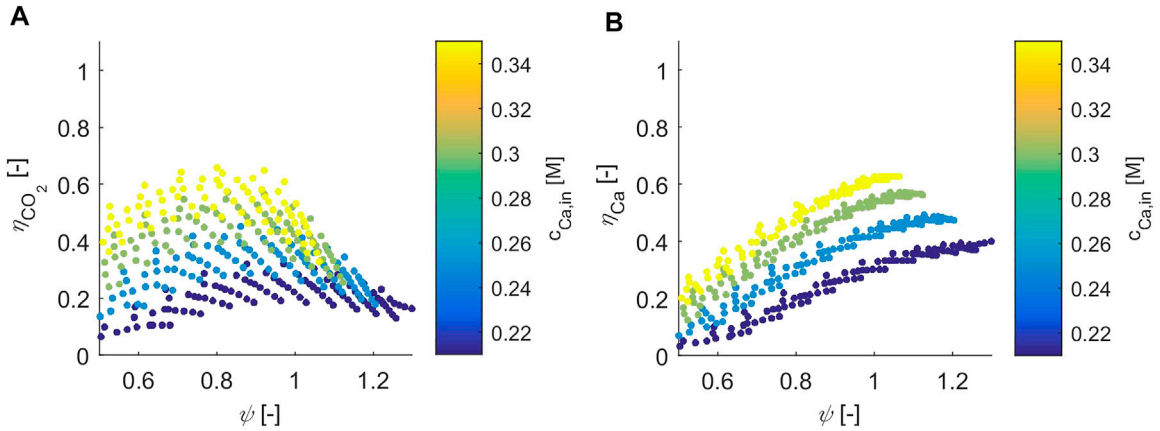

FIGURE 4 | The CO_2 capture efficiency (subplot **(A)**) and the calcium precipitation efficiency (subplot **(B)**) are plotted as a function of ψ. The colors indicate the calcium concentration, read out at the color bar. **(A)** CO_2 capture efficiency. **(B)** Ca precipitation efficiency.

4.2.2 Efficiency of $CaCO_3$ Precipitation Reaction

As CO_2 is absorbed, it speciates into bicarbonate and carbonate ions first, and either exits the reactor with the mother liquer or it reacts with calcium and precipitates as calcium carbonate. **Figure 4** visualizes the calculated values of η_{CO_2} and η_{Ca} as a function of ψ. For a fixed calcium concentration, η_{CO_2} exhibits a broad range of values. As ψ increases, the capture efficiency tends to increase slightly, passes through a maximum and decreases again. If one fixes ψ, the capture efficiency increases with increasing $c_{Ca,in}$ (**Figure 4A**). Moreover, if one multiplies the η_{CO_2} by ψ_F, one obtains the calcium precipitation efficiency, visualized in **Figure 3B**. As one increases ψ, while keeping the $c_{Ca,in}$ constant (e.g., following the yellow points), η_{Ca} increases monotonically. At ψ of about one, the calcium precipitation efficiency seems to reach a plateau. Interestingly, one can see that the capture efficiency peaks at a ψ value smaller than one, while the η_{Ca} exhibits its maximum at ψ equal to one. Summarizing, both ψ and $c_{Ca,in}$ constitute effective quantities, directly correlated to operating variables, to optimizing the process with respect to the CO_2 capture efficiency and to the Calcium precipitation efficiency.

4.2.3 Liquid Speciation: Supersaturation and pH

So far, the effect of the gas flow rate and of the stoichiometry of the feed on the CO_2 absorption efficiency as well as the effect of the calcium concentration on the CO_2 capture and precipitation efficiency have been investigated. The model also allows to compute quantities that are not accessible experimentally, or at least not easily accessible, hence that have not been measured in the experimental campaign, e.g. the supersaturation of the solution, S, and the pH. In this scope, S is studied since it is the driving force for crystal nucleation and growth (it is worth reminding that S is calculated with respect to the solubility of calcite, and that the formation of different polymorphs is not described by the model for the sake of simplicity). Moreover, the pH is an important indicator of key features of the speciation, e.g., the alkalinity of the solution which gives an immediate indication whether the bicarbonate ion or the carbonate ion is dominating.

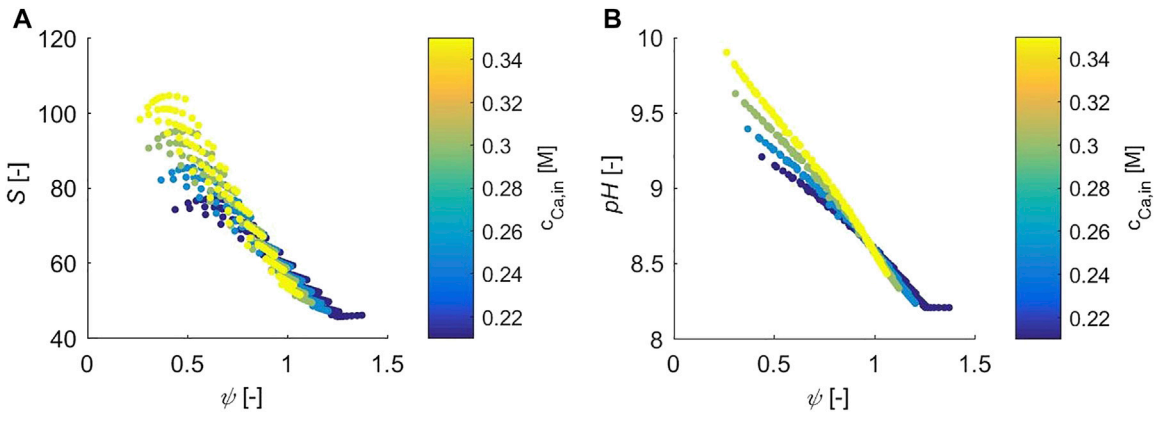

FIGURE 5 | S and the pH are plotted as a function of ψ. The color indicates the calcium concentration. **(A)** S vs. ψ. **(B)** pH vs. ψ.

Figure 5A visualizes the supersaturation as a function of ψ. At low ψ, the supersaturation exhibits values between 70 and 105. As ψ increases, this band of values becomes narrower. Moreover, at low ψ, the supersaturation increases with the calcium concentration, while exactly opposite results have been obtained for ψ larger than one.

Figure 5B shows the pH of the aqueous solution as a function of ψ. The colors indicate the calcium concentration. As expected, the pH also shows a cross-over at a ψ equal to one. It is remarkable that for a fixed calcium concentration, all operating points fall on a single line. As ψ increases, the alkalinity of the solution is reduced, which results in a decreasing value of the pH. The pH values computed are typical for aqueous solutions supersaturated in calcite and vaterite (Chang et al., 2017).

4.2.4 Particle Size

Figures 6A,B visualize the average particle size L_{50} as a function of ψ. As discussed previously (**Figure 6D**, grey points), experiments exhibit a general trend whereby the particle size increases monotonically with ψ. At a fixed ψ value, smaller calcium concentration levels yield smaller particles (**Figure 6A**). Moreover, at a fixed ψ, low liquid feed rates generate larger particles (**Figure 6B**). This is expected, since the residence time is proportional to the reciprocal of Q_{in}. Long residence times usually lead to more particle growth and thus larger particles. Indeed, the solid line in **Figure 6D** was obtained by keeping all parameters constant, while decreasing Q_{in}. Under these circumstances, the model can reproduce the experimental increase of particle size with increasing residence time, also observed in **Figure 6B**.

Finally, **Figure 6C** visualizes L_{50} as a function of S. We observe, that for a fixed value of $c_{Ca,in}$, all points collapse on a line. Thus, at constant $c_{Ca,in}$, L_{50} can be directly related to the supersaturation, S, only. Moreover, at a constant value of S, an increase in the calcium feed concentration yields larger particles. Summarizing, the particle size can be tuned by selecting the corresponding values of Q_{in} and $c_{Ca,in}$.

5 CONCLUDING REMARKS

In this publication, we have developed a reactor model of a continuous crystallizer for the precipitation of calcium carbonate. The product, solid calcium carbonate, is the product of the reaction of a calcium ion with a carbonate ion followed by its transfer to the solid phase at supersaturated conditions. While the calcium is fed with the aqueous solution, CO_2 is fed as a gas to the reactor, absorbs to the solution, speciates into various ions and

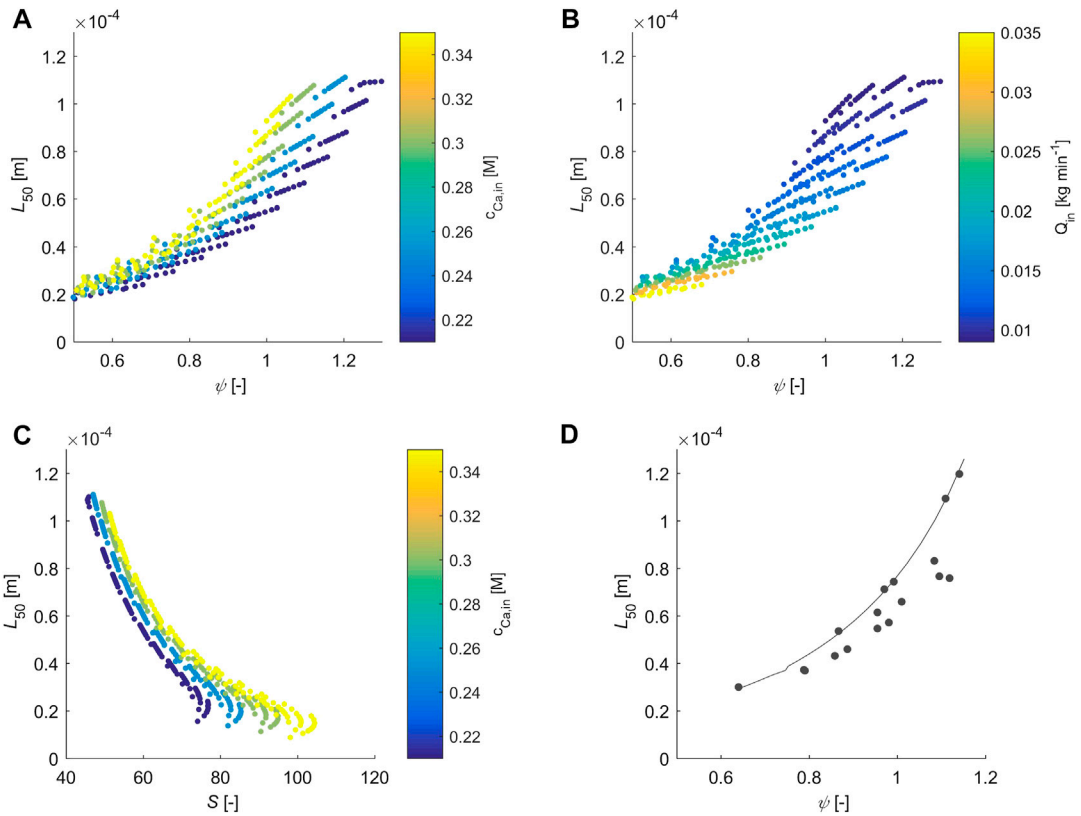

FIGURE 6 | L_{50} is plotted over Ψ and S. The filled cirles in subplot a-c correspond to simulated points, whereas the color represents the quantity specified in the with the color bar. Subplot d shows experimental results (grey circles) and modelling results (solid line), which was obtained by fixing the gas inlet flow rate to 18.5 mmol min^{-1}, the calcium concentration of the feed to 0.3 molal and by varying the liquid feed rate.

reacts with calcium. In order to obtain a precise description of this three-phase system, the model has to consider the thermodynamics of the system and the mechanisms of the kinetic steps of the process. The core of the model is represented by a thermodynamic description of the aqueous solution, considering the dominant reactions, as well as kinetic expressions for the rate of CO_2 mass transfer and the rate of solid formation. These expressions are embedded into material balances for the gas, liquid and solid phase—obtaining a system of equations which can be solved numerically.

In a next step, system specific empirical parameters, which are an integral part of the kinetic rate expressions, have been estimated making use of experimental data obtained in previously published experiments. In specific, the rate of CO_2 mass transfer, the rate of solid formation and the volume weighted average particle size have been used for the parameter estimation. The experimentally and simulated rate of CO_2 mass transfer show a very high quantitative agreement, while the simulated results of the rate of solid formation show a reasonal agreement with experimental results. Surprisingly, and despite its empirical nature and its relative simplicity, the model manages to describe the particle size rather well—although certain mechanism which conventionally affect the particle size, such as particle agglomeration, are not considered by the model. Furthermore, we identified with the help of the model that primary nucleation is dominant over secondary nucleation. This may sound counter intuitive, however the combined effect of the formation of small primary particles and of the occurrence of high supersaturation levels makes such conclusion plausible.

The model was used to compute many potential operating points in order to obtain an in-depth insight into the mechanisms of the process. Results show, that while the CO_2 absorption efficiency is mainly effected by the feed stoichiometry and the gas feed rate, the CO_2 capture and Ca precipitation efficiency exhibit the highest sensitivity towards the calcium concentration of the feed and the ratio of reactants in the aqueous solution. As expected, the liquid feed rate, indirectly proportional to the residence time of the suspension in the aqueous solution, is indirectly proportional to the particle size. Moreover, there is a strong dependency between the particle size and the supersaturation in solution, where a higher supersaturation yields smaller particles, and *vice versa*.

The obtained results—a good description of the rates as well as of the particle properties—is very encouraging, not the least because relatively simple empirical expressions manage to describe a highly complex process. Our work did not stop with the development of the presented model. At the time being, there is an Innosuisse supported and a Horizon 2020 project, which have the aim to advance the maturity of the technology towards TRL 7. In the scope of this projects, concrete fines as well as other alkaline industrial minerals will serve as a source for calcium. The use of such a model helps to design and conduct targeted experimental campaigns, which contribute to enhance the maturity and the potential of the process. Moreover, the reactor model will be an integral part of an overall process model—which is currently under development—describing a novel pH swing process circulating an aqueous solution between a dissolution and a precipitation reactor and accomplishing the so called indirect carbonation of a Ca-bearing precursor, e.g., powder obtained from recycled concrete. The model will be used to conduct a techno-economic and environmental assessment of the new technology.

NOVELTY—CONTRIBUTION TO SCIENTIFIC LITERATURE

- Advanced model of a continuous carbonation reactor with a gas-liquid and solid rate.
- Comparison of primary and secondary nucleation in the space of CO_2 mineralization.
- Combining both CO_2 absorption and crystal growth knowhow for developing a carbonation reactor model.

DATA AVAILABILITY STATEMENT

The original contributions presented in the study are included in the article/**Supplementary Material**, further inquiries can be directed to the corresponding author.

AUTHOR CONTRIBUTIONS

JT conducted the work presented and wrote the manuscript. MM was involve in many detailed discussions about the content of the manuscript, reviewing and editing it.

FUNDING

This research was partially funded by the Swiss Competence Centre for Energy Research—Efficiency Industrial Processes and partially by ETH Zurich.

ACKNOWLEDGMENTS

The authors would like to acknowledge the Swiss Competence Centre for Energy Research—efficiency industrial processes for founding the research activities on this topic. Besides that, we want to thank the ETH Zurich and thus the Swiss Federation for enabling such a research environment without limits. Beyond that, I want to thank Daniel Trottmann for his advice and hands-on support in constructing the setup, Sarah Kienast and Markus Huber

for supporting me with the analytics and my predecessors Mischa Repmann and Subrahmaniam Hariharan for preparing the ground for these research activities. Furthermore, I want to thank Jose Francisco Perez Calvo giving me a hand in developing the CO_2 absorption model.

REFERENCES

Abanades, J. C., Rubin, E. S., Mazzotti, M., and Herzog, H. J. (2017). On the Climate Change Mitigation Potential of CO_2 Conversion to Fuels. *Energy Environ. Sci.* 10 (12), 2491–2499. doi:10.1039/c7ee02819a

Alvarez, A. J., Singh, A., and Myerson, A. S. (2011). Crystallization of Cyclosporine in a Multistage Continuous MSMPR Crystallizer. *Cryst. growth & Des.* 11 (10), 4392–4400. doi:10.1021/cg200546g

Anantharaman, R. B., and David, B. (2017). *CEMCAP Framework for Comparative Techno-Economic Analysis of CO_2 Capture from Cement Plants*.

Becattini, V., Gabrielli, P., and Mazzotti, M. (2021). Role of Carbon Capture, Storage, and Utilization to Enable a Net-Zero-CO_2-Emissions Aviation Sector. *Ind. Eng. Chem. Res.* 60 (18), 6848–6862. doi:10.1021/acs.iecr.0c05392

Brečević, L. (2007). *On Calcium Carbonates: From Fundamental Research to Application*. Zagreb, Croatia: CROATICA CHEMICA ACTA.

Chang, R., Choi, D., Kim, M. H., and Park, Y. (2017). Tuning Crystal Polymorphisms and Structural Investigation of Precipitated Calcium Carbonates for CO_2 Mineralization. *ACS Sustain. Chem. Eng.* 5 (2), 1659–1667. doi:10.1021/acssuschemeng.6b02411

Chen, P.-C., Tai, C. Y., and Lee, K. (1997). Morphology and Growth Rate of Calcium Carbonate Crystals in a Gas-Liquid-Solid Reactive Crystallizer. *Chem. Eng. Sci.* 52 (21-22), 4171–4177. doi:10.1016/s0009-2509(97)00259-5

Darde, V., van Well, W. J. M., Fosboel, P. L., Stenby, E. H., and Thomsen, K. (2011). Experimental Measurement and Modeling of the Rate of Absorption of Carbon Dioxide by Aqueous Ammonia. *Int. J. Greenh. Gas Control* 5 (5), 1149–1162. doi:10.1016/j.ijggc.2011.07.008

Davey, R. G., J. (2000). *From Molecules to Crystallizers*. Manchester: Oxford Chemistry Primers.

Durmaz, T. (2018). The Economics of CCS: Why Have CCS Technologies Not Had an International Breakthrough? *Renew. Sustain. Energy Rev.* 95, 328–340. doi:10.1016/j.rser.2018.07.007

Flaten, E. M., Seiersten, M., and Andreassen, J.-P. (2009). Polymorphism and Morphology of Calcium Carbonate Precipitated in Mixed Solvents of Ethylene Glycol and Water. *J. Cryst. Growth* 311 (13), 3533–3538. doi:10.1016/j.jcrysgro.2009.04.014

Furre, A.-K., Eiken, O., Alnes, H., Vevatne, J. N., and Kiær, A. F. (2017). 20 Years of Monitoring CO_2-injection at Sleipner. *Energy procedia* 114, 3916–3926. doi:10.1016/j.egypro.2017.03.1523

Gardarsdottir, S., De Lena, E., Romano, M., Roussanaly, S., Voldsund, M., Pérez-Calvo, J.-F., et al. (2019). Comparison of Technologies for CO_2 Capture from Cement Production-Part 2: Cost Analysis. *Energies* 12 (3), 542. doi:10.3390/en12030542

Hariharan, S. B. (2017). The Kinetics of CO_2 Mineralization Processes Using Thermally Activated Serpentine. *Diss. ETH No.* 24211.

Hariharan, S., and Mazzotti, M. (2017). Growth Kinetics of Synthetic Hydromagnesite at 90 °C. *Cryst. Growth & Des.* 17 (1), 317–327. doi:10.1021/acs.cgd.6b01546

Hariharan, S., and Mazzotti, M. (2017). Kinetics of Flue Gas CO_2 mineralization Processes Using Partially Dehydroxylated Lizardite. *Chem. Eng. J.* 324, 397–413. doi:10.1016/j.cej.2017.05.040

Hariharan, S., Repmann-Werner, M., and Mazzotti, M. (2016). Dissolution of Dehydroxylated Lizardite at Flue Gas Conditions: III. Near-Equilibrium Kinetics. *Chem. Eng. J.* 298, 44–54. doi:10.1016/j.cej.2016.03.144

IEA (2018). *Low-Carbon Transition in the Cement Industry*. Geneva: Technology Roadmap.

Initiative, G. C. (2016). *Global Roadmap for Implementing CO_2 Utilization*. USA: University of Michigan.

Institute, G. C. (2019). *Global Status of CCS 2019*.

IPCC (2005). *Carbon Dioxide Captuture and Storage*.

IPCC (2018). *Global Warming of 1.5°C*. Special report.

IPCC (2019). *Summary for Policymakers. in: Climate Change and Land: An IPCC Special Report on Climate Change, Desertification, Land Degradation, Sustainable Land Management, Food Security, and Greenhouse Gas Fluxes interrestrial Ecosystems*.

IPCC (2014). *SynthesisReport: Summary for Policymakers*. Geneva: Fifth Assessment Report.

Janssens-Maenhout, G., Crippa, M., Guizzardi, D., Muntean, M., Schaaf, E., Dentener, F., et al. (2017). *Global Atlas of the Three Major Greenhouse Gas Emissions for the Period 1970-2012*. Earth System Science Data. **essd-2017-79**.

Jun, Y.-S., Kim, D., and Neil, C. W. (2016). Heterogeneous Nucleation and Growth of Nanoparticles at Environmental Interfaces. *Acc. Chem. Res.* 49 (9), 1681–1690. doi:10.1021/acs.accounts.6b00208

Jung, W. M., Kang, S. H., Kim, W.-S., and Choi, C. K. (2000). Particle Morphology of Calcium Carbonate Precipitated by Gas-Liquid Reaction in a Couette-Taylor Reactor. *Chem. Eng. Sci.* 55 (4), 733–747. doi:10.1016/s0009-2509(99)00395-4

Kazmierczak, T. F., Tomson, M. B., and Nancollas, G. H. (1982). Crystal Growth of Calcium Carbonate. A Controlled Composition Kinetic Study. *J. Phys. Chem.* 86 (1), 103–107. doi:10.1021/j100390a020

Laakkonen, M. (2005). Local Bubble Size Distributions, Gas–Liquid Interfacial Areas and Gas Holdups in a Stirred Vessel with Particle Image Velocimetry. *Chem. Eng. J.* 109 (1-3), 37–47. doi:10.1016/j.cej.2005.03.002

Last, W., and Stichlmair, J. (2002). Determination of Mass Transfer Parameters by Means of Chemical Absorption. *Chem. Eng. Technol.* 25 (4), 385–391. doi:10.1002/1521-4125(200204)25:4<385::aid-ceat385>3.0.co;2-l

Levenspiel, O. (1999). *Chem. React. Eng.*, 523–539.

Levenspiel, O. (1999). Chemical Reaction Engineering. *Ind. Eng. Chem. Res.* 38 (11), 4140–4143. doi:10.1021/ie990488g

Mac Dowell, N., Fennell, P. S., Shah, N., and Maitland, G. C. (2017). The Role of CO_2 Capture and Utilization in Mitigating Climate Change. *Nat. Clim. Change* 7 (4), 243–249. doi:10.1038/nclimate3231

Maeda, M., and Kato, K. (1995). Dissociation Constants of Ammonium Ion and Activity Coefficients of Ammonia in Ammonium Nitrate Solutions. *J. Chem. Eng. Data* 40 (1), 253–256. doi:10.1021/je00017a054

Mattila, H.-P., Hudd, H., and Zevenhoven, R. (2014). Cradle-to-gate Life Cycle Assessment of Precipitated Calcium Carbonate Production from Steel Converter Slag. *J. Clean. Prod.* 84, 611–618. doi:10.1016/j.jclepro.2014.05.064

Mattila, H.-P., and Zevenhoven, R. (2014). Design of a Continuous Process Setup for Precipitated Calcium Carbonate Production from Steel Converter Slag. *ChemSusChem* 7 (3), 903–913. doi:10.1002/cssc.201300516

Mattila, H.-P., and Zevenhoven, R. (2014). "Production of Precipitated Calcium Carbonate from Steel Converter Slag and Other Calcium-Containing Industrial Wastes and Residues," in *Advances in Inorganic Chemistry* (Elsevier), 347–384. doi:10.1016/b978-0-12-420221-4.00010-x

Nancollas, G. H., and Reddy, M. M. (1971). The Crystallization of Calcium Carbonate. II. Calcite Growth Mechanism. *J. colloid interface Sci.* 37 (4), 824–830. doi:10.1016/0021-9797(71)90363-8

Nations, U. (2015). *Paris Agreement*.

Nehrke, G., Reichart, G. J., Van Cappellen, P., Meile, C., and Bijma, J. (2007). Dependence of Calcite Growth Rate and Sr Partitioning on Solution Stoichiometry: Non-kossel Crystal Growth. *Geochimica Cosmochimica Acta* 71 (9), 2240–2249. doi:10.1016/j.gca.2007.02.002

Ostovari, H., Sternberg, A., and Bardow, A. (2020). *Rock 'n'use of CO 2: Carbon Footprint of Carbon Capture and Utilization by Mineralization*. Achen: Sustainable Energy & Fuels.

Pinsent, B. R. W., Pearson, L., and Roughton, F. J. W. (1956). The Kinetics of Combination of Carbon Dioxide with Ammonia. *Trans. Faraday Soc.* 52, 1594–1598. doi:10.1039/tf9565201594

SUPPLEMENTARY MATERIAL

The Supplementary Material for this article can be found online at: https://www.frontiersin.org/articles/10.3389/fceng.2022.849988/full#supplementary-material

Pohorecki, R., and Moniuk, W. (1988). Kinetics of Reaction between Carbon Dioxide and Hydroxyl Ions in Aqueous Electrolyte Solutions. *Chem. Eng. Sci.* 43 (7), 1677–1684. doi:10.1016/0009-2509(88)85159-5

Puxty, G., Rowland, R., and Attalla, M. (2010). Comparison of the Rate of CO_2 Absorption into Aqueous Ammonia and Monoethanolamine. *Chem. Eng. Sci.* 65 (2), 915–922. doi:10.1016/j.ces.2009.09.042

Ramkrishna, D. (2000). *Population Balances: Theory and Applications to Particulate Systems in Engineering*. Elsevier.

Reis, M. C., Sousa, M. F. B., Alobaid, F., Bertran, C. A., and Wang, Y. (2018). A Two-Fluid Model for Calcium Carbonate Precipitation in Highly Supersaturated Solutions. *Adv. Powder Technol.* 29 (7), 1571–1581. doi:10.1016/j.apt.2018.03.022

Said, A., Laukkanen, T., and Järvinen, M. (2016). Pilot-scale Experimental Work on Carbon Dioxide Sequestration Using Steelmaking Slag. *Appl. energy* 177, 602–611. doi:10.1016/j.apenergy.2016.05.136

Sanna, A., Uibu, M., Caramanna, G., Kuusik, R., and Maroto-Valer, M. M. (2014). A Review of Mineral Carbonation Technologies to Sequester CO_2. *Chem. Soc. Rev.* 43 (23), 8049–8080. doi:10.1039/c4cs00035h

Sutter, D., Van der Spek, M., and Mazzotti, M. (2019). 110th Anniversary: Evaluation of CO_2-based and CO_2-free Synthetic Fuel Systems Using a net-zero-CO2-emission Framework. *Ind. Eng. Chem. Res.* 58 (43), 19958–19972. doi:10.1021/acs.iecr.9b00880

Thomsen, K., and Rasmussen, P. (1999). Modeling of Vapor-Liquid-Solid Equilibrium in Gas-Aqueous Electrolyte Systems. *Chem. Eng. Sci.* 54 (12), 1787–1802. doi:10.1016/s0009-2509(99)00019-6

Tiefenthaler, J., and Mazzotti, M. (2021). *Frontiers in Chemical Engineering*. submitted.Experimental Investigation of a Continuous Carbonation Reactor for $CaCO_3$ Precipitation

Tiefenthaler, J. (2021). Technological Demonstration and Life Cycle Assessment of a Negative Emission Value Chain in the Swiss Concrete Sector. *Front. Clim.* 3 (128). doi:10.3389/fclim.2021.729259

Versteeg, G. F., and Van Swaaij, W. P. M. (1988). Solubility and Diffusivity of Acid Gases (Carbon Dioxide, Nitrous Oxide) in Aqueous Alkanolamine Solutions. *J. Chem. Eng. Data* 33 (1), 29–34. doi:10.1021/je00051a011

Vučak, M. (2002). A Study of Carbon Dioxide Absorption into Aqueous Monoethanolamine Solution Containing Calcium Nitrate in the Gas–Liquid Reactive Precipitation of Calcium Carbonate. *Chem. Eng. J.* 87 (2), 171–179.

Werner, M., Hariharan, S., Zingaretti, D., Baciocchi, R., and Mazzotti, M. (2014). Dissolution of Dehydroxylated Lizardite at Flue Gas Conditions: I. Experimental Study. *Chem. Eng. J.* 241, 301–313. doi:10.1016/j.cej.2013.12.057

Werner, M., Hariharan, S., and Mazzotti, M. (2014). Flue Gas CO_2 Mineralization Using Thermally Activated Serpentine: from Single- to Double-step Carbonation. *Phys. Chem. Chem. Phys.* 16 (45), 24978–24993. doi:10.1039/c4cp02786h

Wolery, T. (2002). *EQ3/6 - Software for Geochemical Modeling Version 8.0, UCRL-CODE-2003-009*. Livermore, California: Lawrence Livermore National Laboratory.

Wolthers, M., Nehrke, G., Gustafsson, J. P., and Van Cappellen, P. (2012). Calcite Growth Kinetics: Modeling the Effect of Solution Stoichiometry. *Geochimica Cosmochimica Acta* 77, 121–134. doi:10.1016/j.gca.2011.11.003

Zeng, Q., Guo, Y., Niu, Z., and Lin, W. (2011). Mass Transfer Coefficients for CO_2 Absorption into Aqueous Ammonia Solution Using a Packed Column. *Ind. Eng. Chem. Res.* 50 (17), 10168–10175. doi:10.1021/ie101821b

Conflict of Interest: JT: PhD student in the Separation Processes Laboratory at ETH Zurich and Co-founder, member of the board and shareholder of the ETH-Spinoff neustark, which aims at scaling up and commercializing the presented technology. MM: Professor of the Separation Processes Laboratory at ETH Zurich and member of the advisory board of the ETH-Spinoff neustark.

Publisher's Note: All claims expressed in this article are solely those of the authors and do not necessarily represent those of their affiliated organizations, or those of the publisher, the editors and the reviewers. Any product that may be evaluated in this article, or claim that may be made by its manufacturer, is not guaranteed or endorsed by the publisher.

NOMENCLATURE

a_{eff} effective interfacial area (m^2/m^3)

a_i activity of aqueous solute *i* (-)

A pre exponential factor of the nucleation rate ($1/m^3/s$)

b number of experiments (-)

$c_{i,in}$ apparent (or total) concentration of aqueous solute *i* entering the reactor (mol/kg)

c_i apparent (or total) concentration of aqueous solute i in the reactor (mol/kg)

D_A diffusivity of component A (m^2/s)

E enhancement factor (-)

E_i enhancement factor for infinitely fast reaction (-)

$f(L)$ particle size distribution ($1/m^4$)

f_{CO_2} fugacity of CO_2 (bar)

F_{in} molar flow rate of the gas entering the reactor (mol/s)

F_{out} molar flow rate of the gas exiting the reactor (mol/s)

f_{MT} CO_2 capture rate ($mol/s/m^3$)

G growth rate (m/s)

H_{CO_2} Henry constant (bar kg/mol)

I ionic strength (mol/kg)

J rate of particle nucleation ($1/m^3/s$)

k_A reaction rate constant of component *A* ($m^3/mol/s$)

k_B Boltzmann constant (m^2 $kg/s^2/K$)

k_c growth rate constant (m/s)

K_i equilibrium constant (-)

k_L liquid phase mass transfer coefficient (m/s)

K_{SP} solubility product of calcite (-)

k_V volume shape factor (-)

L characteristic length of calcite particle (m)

ψ_F molar ratio of carbon to calcium feed rate (-)

ψ effective ratio of reactants in liquid phase (-)

$M_{\mathbf{CaCO_3}}$ molar mass of calcite (kg/mol)

M_H Hatta number (-)

m_w mass of water in the reactor (kg)

$n_{\mathbf{CaCO_3}}$ total number of moles of $CaCO_3$ in the reactor suspension (mol)

n stirring rate

n_{tot} total number of moles of gas in reactor overhead (mol)

P total pressure (Pa)

Q, Q_{in} flow rate of aqueous solution (kg/s)

R ideal gas constant (J/mol/K)

r_{min} rate of limiting reactant ($mol/s/m^3$)

r_c precipitation rate ($mol/s/m^3$)

S_c supersaturation with respect to calcite (-)

T temperature of the aqueous solution (K)

t time (min)

V_R volume of the reactor (m^3)

V_s volume of the liquid phase (m^3)

y_i mole fraction of component *i* in the reactor gas phase (-)

$y_{i,in}$ mole fraction of component *i* in the gas entering the reactor (-)

$y_{i,out}$ mole fraction of component *i* in the gas exiting the reactor (-)

z_i charge of the ion *i* (-)

$\boldsymbol{\tau}$ residence time of the aqueous solution (s)

η_{CO_2} CO_2 mineralization efficiency (-)

$\eta_{CO_2,\,abs.}$ CO_2 absorption efficiency (-)

η_{Ca} precipitation efficiency of Ca (-)

$\alpha\,\beta\,\gamma\,\Delta$ parameter (-)

P density of the solution ($kg\ H_2O/m^3$)

$\boldsymbol{\rho_c}$ density of calcite (kg/m^3)

σ surface energy of $CaCO_3$ (N/m)

ϑ molecular volume of $CaCO_3$ (m^3)

γ_i activity coefficient of ion or molecule *i* (1/M)

μ_2 2nd moment (m^2 crystal/m^3 aqueous solution)

μ_3 3rd moment (m^3 crystal/m^3 aqueous solution)